A Switch in the Kinase Domain of Rat Testis 6-Phosphofructo-2-kinase/Fructose-2,6-bisphosphatase[†,‡]

Mi Ha Yuen,[§] Xiao-li Wang,[||,⊥] Hiroyuki Mizuguchi,[||,⊥] Kosaku Uyeda,[||,⊥] and Charles A. Hasemann*[,§,⊥]

Departments of Internal Medicine and Biochemistry, University of Texas Southwestern Medical Center, 5323 Harry Hines Boulevard, Dallas, Texas 75235, and Research Service, Veterans' Affairs Medical Center, 4500 South Lancaster Road, Dallas, Texas 75216

Received June 3, 1999; Revised Manuscript Received July 23, 1999

ABSTRACT: The bifunctional enzyme 6-phosphofructo-2-kinase/fructose-2,6-bisphosphatase plays an essential role in the regulation of glucose metabolism by both producing and degrading Fru-2,6-P_2 via its distinct catalytic activities. The 6-PF-2-K and Fru-2,6-P_2ase active sites are located in separate domains of the enzyme. The kinase domain is structurally related to the superfamily of mononucleotide binding proteins that includes adenylate kinase and the G-proteins. We have determined three new structures of the enzymatic monomer, each with a different ligand in the ATP binding site of the 6-PF-2-K domain (AMP-PNP, PO_4, and water). A comparison of these three new structures with the ATPγS-bound 6-PF-2-K domain reveals a rearrangement of a helix that is dependent on the ligand bound in the ATP binding site of the enzyme. This helix motion dramatically alters the position of a catalytic residue (Lys172). This catalytic cation is analogous to the Arg residue donated by the rasGAP protein, and the Arg residue at the core of the GTP or GDP sensing switch motion seen in the heterotrimeric G-proteins. In addition, a succinate molecule is observed in the Fru-6-P binding site. Kinetic analysis of succinate inhibition of the 6-PF-2-K reaction is consistent with the structural findings, and suggests a mechanism for feedback inhibition of glycolysis by citric acid cycle intermediates. Alterations in the 6-PF-2-K kinetics of several proteins mutated near both the switch and the succinate binding site suggest a mode of communication between the ATP- and F6P binding sites. Together with these kinetic data, these new structures provide insights into the mechanism of the 6-PF-2-K activity of this important bifunctional enzyme.

Fructose-2,6-bisphosphate (Fru-2,6-P_2)[1] is the most potent known activator of phosphofructokinase (PFK) and an inhibitor of fructose-1,6-bisphosphatase (reviewed in refs *1*−*3*). The balance of glycolysis and gluconeogenesis is thus strongly affected by the cytosolic concentration of Fru-2,6-P_2. The bifunctional enzyme 6-phosphofructo-2-kinase/fructose-2,6-bisphosphatase (6-PF-2-K/Fru-2,6-P_2ase) affects glucose metabolism through its ability to both synthesize and degrade Fru-2,6-P_2 via its kinase and phosphatase activities. Our earlier elucidation of the 2.0 Å crystal structure of the rat testis 6-PF-2-K/Fru-2,6-P_2ase isozyme (RT2K-Wo) revealed that the functional form of the enzyme is a head-to-head homodimer of 55 kDa subunits (*4*). The kinase domains are closely associated via a β-sheet interaction across the dimer interface, forming a continuous 12-stranded β-sheet through the dimer. The phosphatase domains share an interface with the kinase domain within a monomer, but have virtually no contacts with the dimer-related kinase or phosphatase domains.

The 6-PF-2K domain topology is homologous to that of the mononucleotide binding protein family (*4*, *5*). This family includes the nucleoside monophosphate (NMP) kinases (i.e., adenylate kinase) (*6*) and the catalytic core of the G-proteins (i.e., ras and $G_{i\alpha1}$) (*7*, *8*). These proteins all possess two conserved sequence motifs, the Walker A motif (GXXGXGKT) and the Walker B motif (ZZZD, Z being hydrophobic). In the 6-PF-2-K domain, these motifs have the following sequences: $_{45}$GLPARGKT$_{52}$ and $_{124}$VAVFD$_{128}$, respectively. The conserved threonine and aspartic acid of these motifs provide two ligands for the octahedral coordination of a Mg^{2+} ion, which is in turn coordinated to the β- and γ-phosphates of ATP. In our RT2K-Wo structure, Mg^{2+}−ATPγS was found bound by these motifs in the 6-PF-2-K domain.

[†] Supported by grants from the Welch Foundation (C.A.H.), the American Heart Association, Texas Affiliate (C.A.H.), the Department of Veterans Affairs (K.U.), and grants from the National Institutes of Health (DK16194 to K.U. and DK52089 to C.A.H.).

[‡] Coordinates for H256A and RT2K-Wo have been deposited with the Protein Data Bank under file names 2bif and 3bif, respectively.

* To whom correspondence should be addressed: Department of Internal Medicine, University of Texas Southwestern Medical Center, 5323 Harry Hines Blvd., Dallas, TX 75235-8884. E-mail: hasemann@howie.swmed.edu.

[§] Department of Internal Medicine, University of Texas Southwestern Medical Center.

[||] Veterans' Affairs Medical Center.

[⊥] Department of Biochemistry, University of Texas Southwestern Medical Center.

[1] Abbreviations: 6-PF-2-K/Fru-2,6-P_2ase, 6-phosphofructo-2-kinase/fructose-2,6-bisphosphatase; Fru-2,6-P_2, fructose 2,6-bisphosphate; F6P, β-D-fructose 6-phosphate; β-OG, octyl β-D-glucopyranoside; PFK, phosphofructokinase; AMP-PNP, 5′-adenylyl imidodiphosphate; RT2K, rat testis isozyme of 6-PF-2-K/Fru-2,6-P_2ase; RT2K-Wo, RT2K with all four tryptophans mutated to phenylalanine; H256A, mutant form of RT2K-Wo with an additional histidine 256 to alanine mutation; RT2K-Wo/$P3_121$, original RT2K-Wo crystal in space group $P3_121$; RT2K-Wo/$C2$, RT2K-Wo crystal in space group $C2$; H256A-A, monomer A in the $P1$ crystal of the H256A mutant; H256A-B, monomer B in the $P1$ crystal of the H256A mutant.

10.1021/bi991268+ CCC: $18.00
Published on Web 08/31/1999

These enzymes share a common catalytic function as well, namely, the transfer of the γ-phosphate of a nucleoside triphosphate to an acceptor molecule (Fru-6-P for 6-PF-2-K, ADP for adenylate kinase, or water for the G-proteins). In many phosphotransferases, the phosphate acceptor molecule is activated by some protein-derived nucleophile, typically an Asp or Glu residue [for example, Asp127 activating the 1-hydroxyl of Fru-6-P in the PFK reaction (*9*, *10*)]. In these adenylate kinase-related enzymes, however, there is no protein-derived nucleophile, and various explanations of the mechanism of phosphotransfer have been presented (*11*−*16*). Both the G-proteins and the 6-PF-2-K domain are very slow catalysts, with turnover rates on the order of two to six per minute. Such slow turnovers are consistent with their in vivo roles as regulatory proteins, rather than enzymes in a metabolic pathway. It is widely accepted that the slow turnover rates are due to the lack of an activating nucleophile (*17*), but there is little consensus on the mechanism of the reaction in the absence of the nucleophile. The G-proteins are the best described, where the opposing views include activation of substrate (water) by glutamine, by substrate (GTP), or by a purely dissociative mechanism with no need for substrate activation. In all three cases, however, the neutralization of charge at the γ-PO_4 and/or $\beta-\gamma$ bridge oxygen of GTP is crucial. This is achieved in the heterotrimeric G-proteins in part by an arginine side chain that is located in one of the switch regions that signal the presence of GTP in the active site (*8*). In the small G-proteins, an analogous arginine is derived from the binding of a GAP protein (*18*, *19*). In the 6-PF-2-K domain, the analogous residue is K172. Mutagenesis data have verified that K172 is a catalytic amino acid for the 6-PF-2-K reaction (*20*). In each case, the role of the positive charge is presumed to be in stabilization of the transition state, though the mechanism that initiates that transition state remains unresolved.

To understand the mechanisms of the 6-PF-2-K and Fru-2,6-P_2ase reactions, we have pursued crystal structures in the presence of different ligands and/or the structures of mutant proteins. The proteins used in this study are mutant forms of the rat testis isoform of 6-PF-2-K/Fru-2,6-P_2ase. RT2K-Wo is a mutant that had all four tryptophan residues replaced with phenylalanine for a fluorescence study, serendipitously resulting in a dramatic increase in the level of expression with no significant change in either the 6-PF-2-K or Fru-2,6-P_2ase activity (*21*). This is the same protein that was used for our initial determination of the RT2K structure (*4*). H256A is a mutant of RT2K-Wo in which the catalytic His256 of the Fru-2,6-P_2ase domain is replaced with alanine. This histidine was previously shown to be the location of a covalent phosphohistidine intermediate in the Fru-2,6-P_2ase reaction (*22*). Surprisingly, replacement of His256 in RT2K-Wo resulted in an enzyme which retained 17% of its Fru-2,6-P_2ase activity (*23*). We have recently published a description of the Fru-2,6-P_2ase domain of this mutant (*24*). We report here a comparison of all the 6-PF-2-K domain structures determined to date, revealing a variety of bound ligands, and an unanticipated rearrangement of a catalytic residue. Several kinetic experiments whose results support the hypotheses derived from this structural information are also presented.

EXPERIMENTAL PROCEDURES

Protein Purification and Crystallization. Homogeneous preparations of both RT2K-Wo and H256A proteins were prepared as described previously (*21*, *25*). All crystals were grown by hanging drop vapor diffusion at 4 °C by employing a modification of the method reported previously (*26*). Crystals of H256A were grown by mixing 10 mg/mL protein [in 50 mM Tris-PO_4 (pH 7.5), 5% glycerol, 40 μM EDTA, 40 μM EGTA, 800 μM DTT, 0.4% PEG 300, 1.7 mM F6P, 1.7 mM AMP-PNP, and 1% octyl β-D-glucopyranoside] in a 1:1 ratio with a well solution of 17% polyethylene glycol 4000, 90 mM succinate (pH 6.0), 10% glycerol, and 10 mM $MgCl_2$. RT2K-Wo crystals were grown by mixing a 10 mg/mL protein solution of RT2K-Wo [in 50 mM Tris-PO_4 (pH 7.5), 5% glycerol, 100 μM EDTA, 10 mM DTT, 0.5% octyl β-D-glucopyranoside, 3 mM F6P, and 1 mM AMP-PNP] in a 1:1 ratio with a well solution of 11% polyethylene glycol 4000, 50 mM succinate (pH 5.5), 50 mM Tris-PO_4 (pH 7.5), 100 μM EDTA, 10 mM DTT, 10% glycerol, and 3 mM $MgCl_2$.

Site-Directed Mutagenesis. Oligonucleotide-directed in vitro mutagenesis was performed as described by Kunkel (*27*), using the Muta-Gene M13 in vitro mutagenesis kit (Bio-Rad). Plasmid RT2K/pT7-7 containing the RT2K gene, cloned in a pT7-7 vector (*28*), was digested with *Xba*I and *Hin*dIII, and the isolated 1.7 kb fragment containing the RT2K gene was ligated into the *Xba*I−*Hin*dIII site of M13mp18 (M13/RT2K). The phage harboring M13/RT2K was transfected into *Escherichia coli* CJ236 cells (dut^- ung^-). The recombinant M13/RT2K phage was purified and used to prepare the uracil-containing single-stranded template. The synthesized double-stranded DNA was used to transform *E. coli* MV1190 cells. Mutant derivatives were identified by DNA sequencing (*29*). The mutant DNAs were digested with *Nde*I and *Hin*dIII, and the DNA fragments containing a mutated RT2K gene were subcloned into the *Nde*I−*Hin*dIII site of pT7-7 (RT2K/pT7-7). The expression plasmids that were obtained were transformed into *E. coli* BL21(DE3) cells, and recombinant mutant enzymes were purified as described above. Before the assay, all enzymes were desalted by column centrifugation (*30*) in 50 mM Tris-PO_4 (pH 7.5) containing 0.5 mM EDTA, 0.5 mM EGTA, 2 mM DTT, 1% polyethylene glycol (M_r = 300), and 5% glycerol.

Assay Method for 6-PF-2-K Activity. The assay is based on the determination of the amount of Fru-2,6-P_2 produced, and is the same as that described previously (*31*) with slight modification. The reaction mixture in a final volume of 50 μL contained 100 mM Tris-HCl (pH 7.5), 0.1 mM EDTA, 1 mM F6P, 1 mM ATP, 5 mM $MgCl_2$, and the indicated amount of succinate. The reaction was initiated by the addition of enzyme, and the reaction mixture was incubated at 30 °C for 10 min. After incubation, the reaction was terminated by the addition of 50 μL of 0.1 N NaOH, and the mixture was incubated at 85 °C for 90 s. Aliquots were assayed for Fru-2,6-P_2 activity as described by Uyeda et al. (*32*). One unit of enzyme activity is defined as the amount of enzyme that catalyzes the formation of 1 μmol of Fru-2,6-P_2 per minute under these conditions.

X-ray Data Collection and Processing. Crystals were prepared for flash-freezing in liquid propane by serial transfer into solutions of surrogate mother liquors with increasing

concentrations of glycerol (10 to 20% in 5% steps). Crystals were maintained at 120 K in a dry nitrogen stream using an Oxford Cryostream Cooling device. Data for H256A were collected on a DIP-2020 image plate detector (MacScience), while data for RT2K-Wo were collected on a DIP-2030 image plate detector (MacScience) mounted on a Rigaku rotating anode generator operated at 50 mA and 100 kV, with double-mirror focusing (MacScience). Diffraction intensities were integrated using the program Denzo (*33*). All data were merged and scaled in Scalepack (*33*) and reformatted for subsequent use in X-PLOR (*34*) or CCP4 (*35*), reserving 10% of the data as a test set for R_{free} calculations (*36*).

Phasing by Molecular Replacement, Model Building, and Refinement. The solution of the H256A structure was previously reported in a description of the Fru-2,6-P_2ase domain of that enzyme (*24*), and its determination proceeded essentially as described here for the solution of the RT2K-Wo/*C*2 crystal. A Patterson rotation search, PC refinement, and a translation search were carried out using the program X-PLOR, using a polyalanine model derived from the RT2K-Wo crystal structure (*4*). The molecular replacement was unambiguous, with a translation function peak 12.5σ above the mean solution, and 9.7σ above the next best solution. Rigid-body minimization of this translation solution using data from 20 to 2.8 Å resolution led to an R_{free} of 0.503 for the polyalanine model, and an R_{free} of 0.391 with all side chains included. To minimize model bias, initial electron density maps were calculated with the polyalanine molecular replacement phases and data from 30 to 2.4 Å, using SIGMAA (*37*) weighting as implemented in X-PLOR. Model rebuilding was achieved using the program O [version 6.1 (*38*)]. The major changes in the structure are related to changes in the ligand-binding state of both catalytic domains, and changes due to crystal packing. Rebuilding and positional and *B*-factor refinement yielded the final model reported here with the indicators of model quality reported in Table 1. Coordinates for H256A and RT2K-Wo have been deposited with the Protein Data Bank (*39*), under file names 2bif and 3bif, respectively. Superposition of coordinates was accomplished using the lsq_explicit and lsq_improve facilities in O (*38*).

RESULTS AND DISCUSSION

Protein Crystallization and Structure Determination. Conditions for the purification and crystallization of the RT2K-Wo and H256A proteins are described in Experimental Procedures, and are similar to our previously reported conditions (*26*). The most significant changes in the conditions for this crystallization are the inclusion of AMP-PNP instead of ATPγS and alterations in the amount and pH of succinate. The H256A crystals belong to space group *P*1 with the following unit cell dimensions: $a = 61.7$ Å, $b = 73.5$ Å, $c = 76.7$ Å, $\alpha = 116.9°$, $\beta = 99.31°$, and $\gamma = 105.2°$, with two monomers (a functional dimer) in the asymmetric unit. The RT2K-Wo crystals belong to space group *C*2 with the following unit cell dimensions: $a = 106.7$ Å, $b = 108.7$ Å, $c = 71.7$ Å, $\alpha = \gamma = 90°$, and $\beta = 129.5°$, with a single monomer in the asymmetric unit. Both of these crystal forms are different from the original RT2K-Wo crystals in space group $P3_121$ (*4*). The H256A and RT2K-Wo/*C*2 crystals diffract to 2.4 and 2.3 Å resolution, respectively. The structures were determined by molecular replacement using the reported RT2K-Wo structure as a search model. Details of the structure solution of RT2K-Wo/*C*2 are presented in Experimental Procedures, while the H256A structure determination was reported previously (*24*). A summary of the qualities of the data and models is presented in Table 1.

Table 1: Structure Determination Statistics

	RT2K-Wo	H256A
Diffraction Data		
space group	*C*2	*P*1
resolution (Å)	30−2.3	30−2.4
no. of reflections [$F \geq \sigma(F)$]	23883	37144
completeness (%)	88.1 (84.9)	95.1 (93.1)
multiplicity	2.64 (2.30)	2.16 (2.14)
$I/\sigma(I)$	36.5 (7.16)	15.6 (4.75)
R_{sym}	3.9	5.2
R_{work}	19.7	20.0
R_{free}	24.3	24.4
Model Composition		
no. of amino acids	432	864
no. of protein atoms	3519	7017
no. of heteroatoms	58	153
no. of waters	187	274
no. of refinement parameters	15056	29776
no. of observations per parameter	1.58	1.25
Stereochemistry		
bond lengths (Å)	0.008	0.012
bond angles (deg)	1.50	1.60
improper angles (deg)	1.26	1.48
Thermal Parameters		
mean *B* for main chains	37.4	33.4
mean *B* for side chains	39.9	35.7
mean *B* for protein and heteroatoms	39.0	34.8
mean *B* for solvent	38.6	27.6
rms deviation for bond lengths	4.08	2.97
rms deviation for bond angles	5.99	4.54
overall *B* (Wilson plot)	39.9	37.4

Overview of the Three Dimer Structures. The overall dimer structures of H256A and the *C*2 form of RT2K-Wo are grossly similar to the original RT2K-Wo structure (RT2K-Wo/$P3_121$) (*4*). Thus, there is close interaction between the 6-PF-2-K domains, with the independent Fru-2,6-P_2ase domains tethered to this 6-PF-2-K dimer. The Fru-2,6-P_2-ase domains of the RT2K-Wo/*C*2 and RT2K-Wo/$P3_121$ structures are essentially identical, with phosphate ions bound in the binding pockets for the 6- and 2-phosphates of Fru-2,6-P_2. Each of the Fru-2,6-P_2ase domains of the H256A monomers has a bound F6P and phosphate ion. On the basis of these structures, we have recently described a model of the Fru-2,6-P_2-bound state of the Fru-2,6-P_2ase domain, and proposed a catalytic mechanism for the Fru-2,6-P_2ase reaction (*24*).

The data presented in this report focus on the 6-PF-2-K domains derived from these three crystals. To date, we have determined the structures of four crystallographically distinct 6-PF-2-K/Fru-2,6-P_2ase monomers. Two monomers are derived from crystals of the RT2K-Wo protein (the previously reported RT2K-Wo/$P3_121$ crystal structure and the RT2K-Wo/*C*2 crystal form reported here). The other two monomers arise as the crystallographically independent views of the H256A mutant protein (monomers H256A-A and H256A-B). What is most different among the four monomer structures is the nature of the ligands bound in their F6P

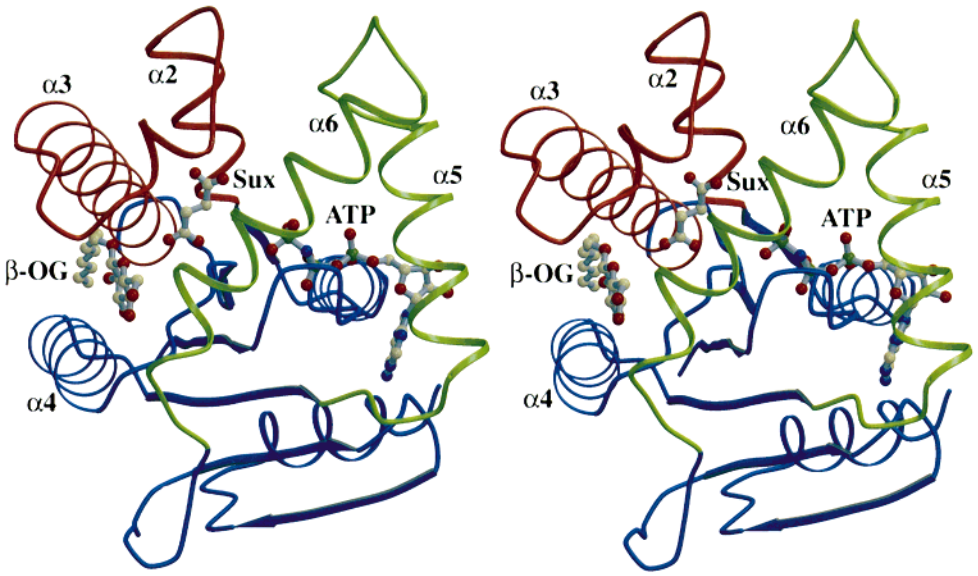

FIGURE 1: 6-PF-2-K domain with bound ligands. A stereo ribbon diagram of the 6-PF-2-K domain of the H256A-A monomer is shown with ligands drawn as ball-and-stick models. The F6P binding loop consisting of helices α2 and α3 and the intervening turn is red. The ATP binding loop consisting of helices α5 and α6 and the intervening turn is green, and the rest of the protein is blue. AMP-PNP is shown bound in the ATP binding site (ATP). Succinate is bound in the F6P binding site (Sux), while a detergent molecule (*β*-OG) is bound with its glucose ring interacting with the backside of the F6P binding site, and its aliphatic tail between helices α3 and α4. All figures were generated with Molscript (*49*) or Bobscript (*50*), and Raster3D (*51*).

Table 2: Ligands in the 6-PF-2-K Domain ATP and F6P Binding Sites

6-PF-2-K domain	ligands bound
H256A-A	ATP site, AMP-PNP/ADP
	F6P site, succinate and *β*-OG
H256A-B	ATP site, PO_4 ion
	F6P site, succinate
RT2K-Wo/*C*2	ATP site, water
	F6P site, succinate and *β*-OG
RT2K-Wo/$P3_121$	ATP site, ATP*γ*S/ADP
	F6P site, empty

and ATP binding sites, and the conformations of the F6P and ATP binding loops in the 6-PF-2-K domains. Figure 1 shows a ribbon diagram of the H256A-A 6-PF-2-K domain. This monomer has three ligands bound to its 6-PF-2-K domain; AMP-PNP in the ATP binding site, succinate in the proposed F6P binding site, and octyl *β*-D-glucopyranoside (*β*-OG) bound near the proposed F6P site. These three ligands are not found in all four 6-PF-2-K domains, but each is found more than once, as summarized in Table 2.

ATP Binding Site. The ligands bound in the ATP binding pocket (P-loop or Walker A motif) of the four 6-PF-2-K domains vary from ATP*γ*S or AMP-PNP, to a single PO_4 ion, to a single water molecule. A majority of the ATP*γ*S and AMP-PNP molecules found in the RT2K-Wo/$P3_121$ and H256A-A structures, respectively, are hydrolyzed to ADP. The occupancies of the *γ*-phosphates were reduced during model refinement to levels that yield *B*-factors consistent with the α- and *β*-phosphates (there are not enough data at ∼2.3 Å resolution to support the refinement of both *B*-factors and occupancies). Thus, the *γ*-phosphate occupancy was estimated to be 40% for ATP*γ*S, and 20% for AMP-PNP. While these occupancy estimates are not rigorous, it is clear from the inspection of electron density maps that the occupancy is lower for H256A-A−AMP-PNP than it is for RT2K-Wo/$P3_121$−ATP*γ*S. The absence of any nucleotide in the 6-PF-2-K domains of the H256A-B and RT2K-Wo/*C*2 monomers reflects a trend in our crystallization trials where the use of AMP-PNP instead of ATP or ATP*γ*S leads to more unstable protein and more difficult crystallization. We have interpreted this to mean that the 6-PF-2-K complex with AMP-PNP is not as stable as that with ATP or ATP*γ*S, at least under the conditions we have surveyed. As seen in the RT2K-Wo/$P3_121$ structure (*4*), there is an intimate interaction between the main chain nitrogens of the P-loop and the *β*−*γ* bridge oxygen of ATP*γ*S. The AMP-PNP *β*−*γ* bridge nitrogen (NH) is likewise forced into an interaction with these same P-loop main chain NH groups. This unfavorable interaction would explain the observed weaker binding of AMP-PNP, the high proportion of ADP found in the ATP binding site of the H256A-A monomer, and the complete lack of nucleotide in the H256A-B and RT2K-Wo/*C*2 6-PF-2-K domains.

F6P Binding Site. The location of the F6P binding site in the 6-PF-2-K domain has been inferred by the overlap of the analogous substrate pocket in the adenylate kinase family, and the location of 6-PF-2-K residues that significantly affect F6P binding when mutated (*4*, *20*, *23*). A succinate molecule (included in the crystallization as a pH ∼6.0 buffer) was unambiguously identified in this presumed F6P binding pocket in three of the four monomers (Table 2). Figure 2 shows the electron density of succinate bound to the H256A-A monomer. The succinate molecule is sandwiched between Arg78 in the F6P binding loop and Thr130 at the base of the F6P binding pocket. Succinate bound in this position gives the impression of a wedge in the jaw of the F6P binding site, which would keep the F6P binding loop from closing completely (see Figure 1). Site-specific mutagenesis and kinetic studies found that replacement of R78 with His or Leu elevated the K_m^{F6P} by 200-fold (*20*). We had previously modeled F6P in the RT2K-Wo/$P3_121$ active site (C. A. Hasemann et al., unpublished data) based on an in-line transfer of phosphate from ATP to the 2-hydroxyl of F6P and the locations of amino acids shown by mutagenesis

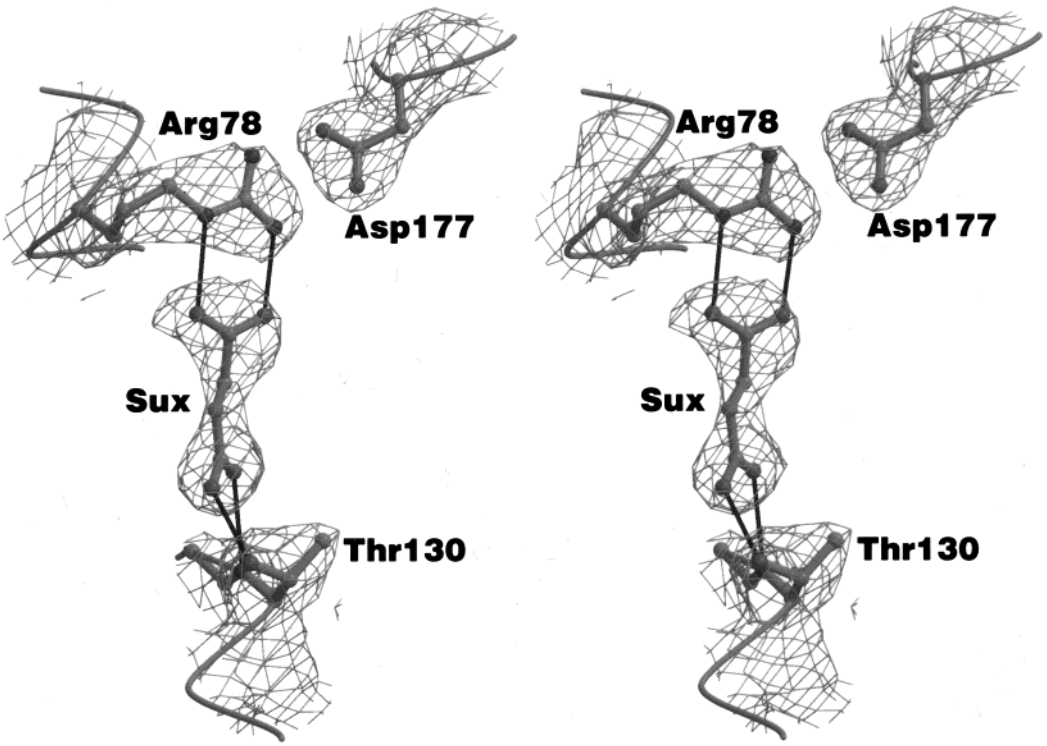

FIGURE 2: Electron density of succinate bound in the F6P binding site. The succinate is bound by Arg78 and both the side chain hydroxyl and main chain nitrogen of Thr130, with the interactions between them represented by solid lines. Succinate (Sux), Thr130, Arg78, and Asp177 are drawn as ball-and-stick models, with a coil trace of the Cα positions in their vicinity. The $2F_o - F_c$ electron density is contoured at 1σ above the mean density.

to affect F6P binding. The succinate and this modeled F6P occupy overlapping positions in the F6P binding site. Thus, succinate bound in this location would clearly interfere with F6P binding. On the basis of this observation, we have tested the succinate inhibition of 6-PF-2-K activity. Succinate is in fact an inhibitor of the 6-PF-2-K reaction with a K_i of 25 μM, comparable to the observed K_M^{F6P} of 40 μM. This finding may suggest a mechanism of feedback inhibition of Fru-2,6-P_2 synthesis (and resultant inhibition of glycolysis) by citric acid cycle intermediates.

We previously acknowledged the presence of residual electron density in the F6P binding site of the RT2K-Wo/$P3_121$ structure that could not be satisfactorily modeled as water (*4*). Since the conditions for the RT2K-Wo/$P3_121$ and RT2K-Wo/*C*2 crystallizations included the same concentration of succinate, we have reinspected the RT2K-Wo/$P3_121$ electron density and attempted refinement with succinate in the F6P binding site. This effort led to the same conclusion, however, that the F6P binding site of the RT2K-Wo/$P3_121$ crystal does not contain any single ligand (and particularly not F6P or succinate) at a significant occupancy that can be modeled and fit to the data.

A molecule of β-OG is bound to the RT2K-Wo/*C*2 and H256A-A monomers, in a position that could be described as the "backside" of the F6P binding site (Figure 1). β-OG is included in the crystallization because it delays the precipitation of the protein induced by PEG. Hydroxyl oxygens in the β-OG glucose ring interact with both Arg102 and Arg136, residues that have a dramatic influence on the binding of F6P (*20*, *40*). We describe this position of the glucose moiety as the backside of the F6P binding site because, while the β-OG interacts with residues that are predicted to interact with the 6-phosphate of F6P, it does so from the outside of the binding site, rather than from the interior of the pocket where succinate is bound. The aliphatic tail of β-OG is inserted into the local hydrophobic core formed between helices α3 and α4. Helix α3 is part of the F6P binding loop, and a small change in the position of this helix relative to RT2K-Wo/$P3_121$ allows the β-OG hydrophobic tail to slip into this location.

Comparison of the Four 6-PF-2-K Domains. Given that all four 6-PF-2-K domains have different bound ligands, it is interesting to examine the overall structural changes among them, and to look for correlations between those changes and the bound ligands. Thus, we chose the ATPγS-bound RT2K-Wo/$P3_121$ domain as a reference, and superimposed on it the other three monomer structures. For each Cα in these three monomers, we then measured the distance (in angstroms) to the equivalent Cα atom in the RT2K-Wo/$P3_1$-21 domain, and plotted these positional differences as a function of sequence position (Figure 3). Peaks in these graphs thus represent regions in the compared 6-PF-2-K domains that differ from the original ATPγS-bound structure. In any such comparison, the role of crystal contacts must be considered, so regions of the 6-PF-2-K domains involved in crystal contacts are indicated. Only two of these contacts appear as significant differences among the structures (regions around positions 83 and 180). The most significant changes instead are concentrated in the F6P and ATP binding loops, and other regions associated with the binding of ATP. Motions in the F6P and ATP binding loops were anticipated (*4*), on the basis of the large-scale motions observed in the analogous loops of adenylate kinase where the ATP and substrate binding loops open and close to bind and release substrates and products (*41*, *42*). The motions we have observed in the 6-PF-2-K domain thus far are much less

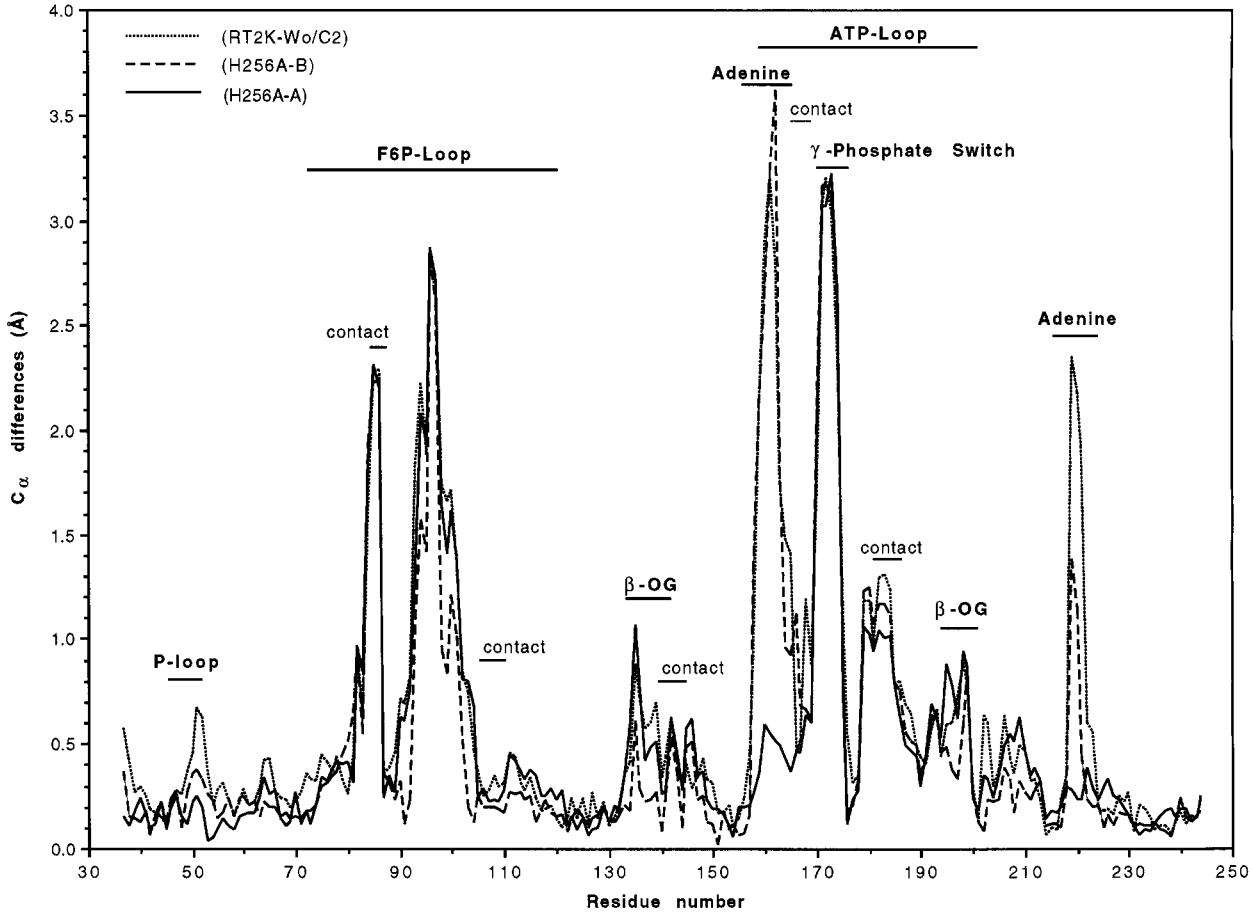

FIGURE 3: Graph of Cα positional differences among the four 6-PF-2-K domains. The differences between the ATPγS-bound structure and the three other 6-PF-2-K domains are made evident in this graph of distances vs sequence position. Each domain was optimally superimposed on the ATPγS structure, and the distance between each Cα pair was plotted for the RT2K-Wo/*C*2 (dotted line), H256A-A (dashed line), and H256A-B (solid line) 6-PF-2-K domains. The largest differences among the structures occur in the F6P and ATP binding loops. Changes due to the absence of the adenine moiety in the RT2K-Wo/*C*2 and H256A-A structures (but remaining similar in the AMP-PNP-bound H256A-B domain) are labeled Adenine. The switch motion due to the absence of a regular γ-phosphate in all three domains is labeled γ-Phosphate Switch. The subtle change in the P-loop due to the absence of any phosphates in the RT2K-Wo/*C*2 structure is noted, as are the small changes due to the binding of β-OG. Changes in the structures that are apparently due to crystal contacts are denoted contact.

dramatic than those described for adenylate kinase, but do reflect an intrinsic mobility of these loops, presumably related to the binding of F6P and ATP and the release of Fru-2,6-P_2 and ADP.

Four regions of the 6-PF-2-K domain exhibit significant structural changes related directly to the nature of the ligand in the ATP binding site. Two of these (labeled Adenine in Figure 3) represent the protein collapsing into the space that would be occupied by the adenine portion of ATP. The third site is in the P-loop, where the empty binding site of the RT2K-Wo/*C*2 domain has induced a reorientation of the P-loop (labeled P-Loop in Figure 3). The rearrangement of the P-loop is presumably due to the changed electrostatic character of this region in the absence of the negative charges provided by the ATPγS, AMP-PNP, and P_i phosphate ion-(s) in the RT2K-Wo/*P*$3_1$21, H256A-A, and H256A-B domains, respectively.

A Switch Motion in the 6-PF-2-K Domain. The fourth region of structural change is a rearrangement of helix α5 (labeled γ-phosphate Switch in Figure 3, and pictured in Figure 4). In the original RT2K-Wo/*P*$3_1$21 structure (*4*), Lys172 was found to interact with the $\beta-\gamma$ bridge oxygen and γ-phosphate of ATPγS as shown in Figure 4a. In each of the new 6-PF-2-K domain structures reported here, Lys172 has swung out of the active site to the opposite side of the helix (as seen in Figure 4b) due to a reorganization of the C-terminal half of the helix. In the ATP-bound state with Lys172 in the active site (Figure 4a), the helix has seven regular α-helical hydrogen bonds (n to $n + 4$), two irregular mixed α/π hydrogen bonds (n to $n + 4$ and $n + 5$), two nonbonded carbonyls, and, finally, a mixed $\alpha/3_{10}$ hydrogen bond (n to $n + 3$ and $n + 4$). In the reorganized helix (Figure 4b), there are 12 regular α-helical hydrogen bonds with no irregularities. These two views of the ATP binding region lead to a description of this switch helix during a catalytic cycle. Upon binding of ATP, Lys172 would be recruited to the active site by its energetically favorable charge interaction with the γ-phosphate and $\beta-\gamma$ bridge oxygen (but not the AMP-PNP bridge nitrogen). In this process of recruiting Lys172 to the active site, energy would be lost (or stored) as the helix is partially unwound (Figure 4a). After transfer of the γ-phosphate to F6P, and the loss of the Lys172$-PO_4$ interaction, the helix would revert to its regular conformation, removing Lys172 from the active site, substituting it with Val171. The substitution of valine for lysine in the active site would in turn promote the dissociation of ADP. This remarkable switch between conformations of Lys172 thus creates an energetic counterbalance that assists in traversing

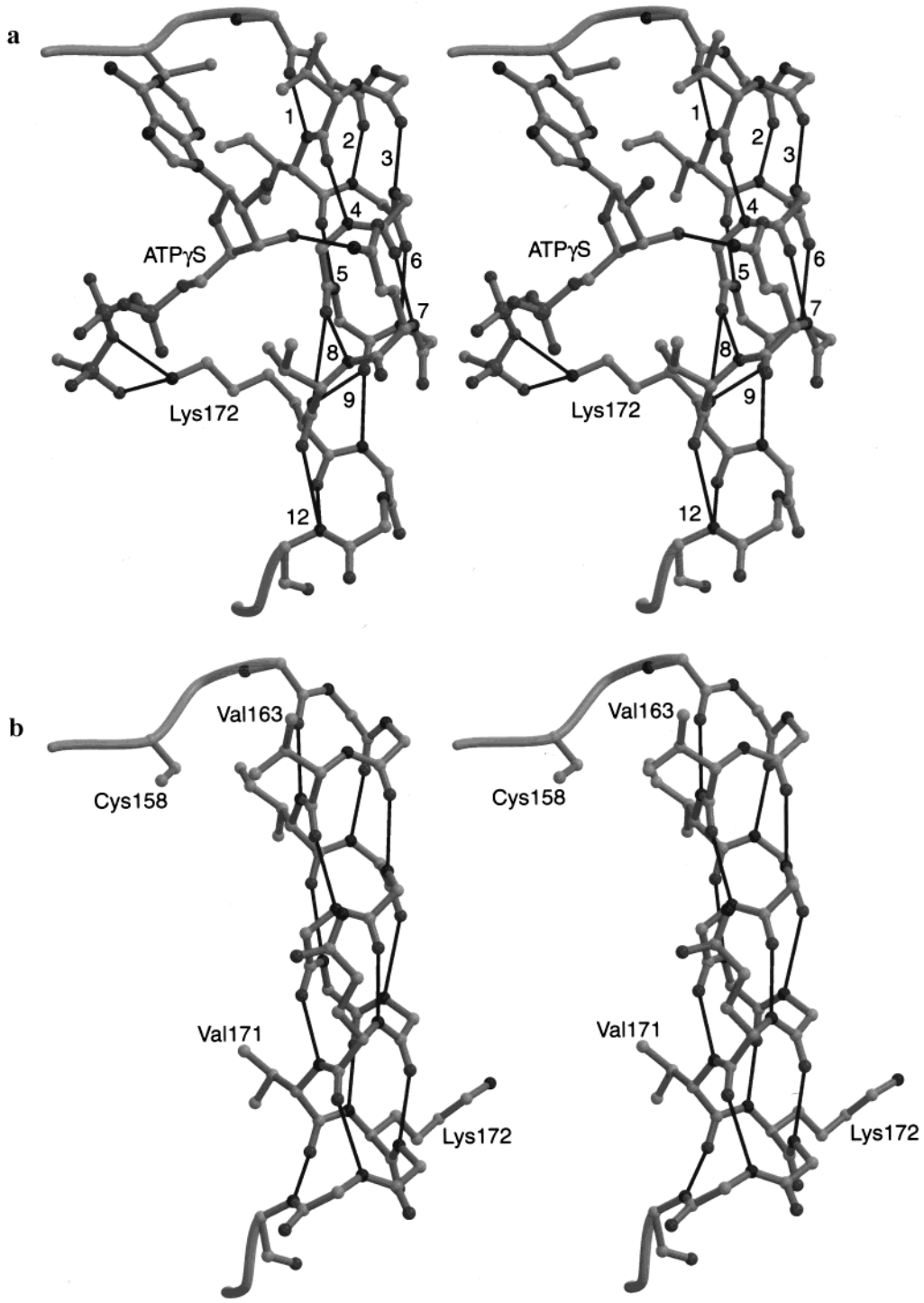

FIGURE 4: Switch helix and Lys172. Stereoviews of the switch helix (helix α5) in the ATP-bound (RT2K-Wo/$P3_121$, a) and unbound (RT2K-Wo/$C2$, b) states are shown here. The helical hydrogen bonds are shown as solid lines between the carbonyl oxygens and amino nitrogens in the main chain, drawn as ball-and-stick representations. In the ATP-bound conformation (a), the helix has seven regular α-helical (n to $n + 4$) hydrogen bonds (numbered 1−7) followed by two irregular mixed α/π (n to $n + 4$ and $n + 5$) hydrogen bonds (numbered 8 and 9), two nonbonded carbonyls (unlabeled), and, finally, a mixed $\alpha/3_{10}$ hydrogen bond (numbered 12). In the reorganized helix (b), there are 12 regular α-helical hydrogen bonds with no irregularities. Due to these changes in hydrogen bonding, a section of the helix including Lys172 undergoes a dramatic conformational change. In the ATP-bound state, Lys172 interacts with the γ-phosphate and $\beta-\gamma$ bridge oxygen, while in the unbound state, Val171 is closest to the ATP binding site while Lys172 has swung entirely out of the binding pocket. Also shown in this figure, Cys158, Val163, and Ile164 alter their positions and/or rotamer configurations in panel b relative to the ATP-bound state, filling the space vacated by the adenine moiety.

the energy barriers to substrate binding and product release. A very different counterbalance mechanism was reported for *E. coli* adenylate kinase, in which the energy of formation of the enzyme−substrate complex is transformed into mobility of loops at the opposite end of the enzyme (*43*).

As we have noted before (*4*), the position of Lys172 in relation to the ATP is similar to that observed for Arg178 in the heterotrimeric G-protein $G_{i\alpha1}$ (*8*), Arg142 in yeast uridylate kinase (*44*), and, more recently, Arg789 from the rasGAP protein in the ras−rasGAP complex (*18*). Data for

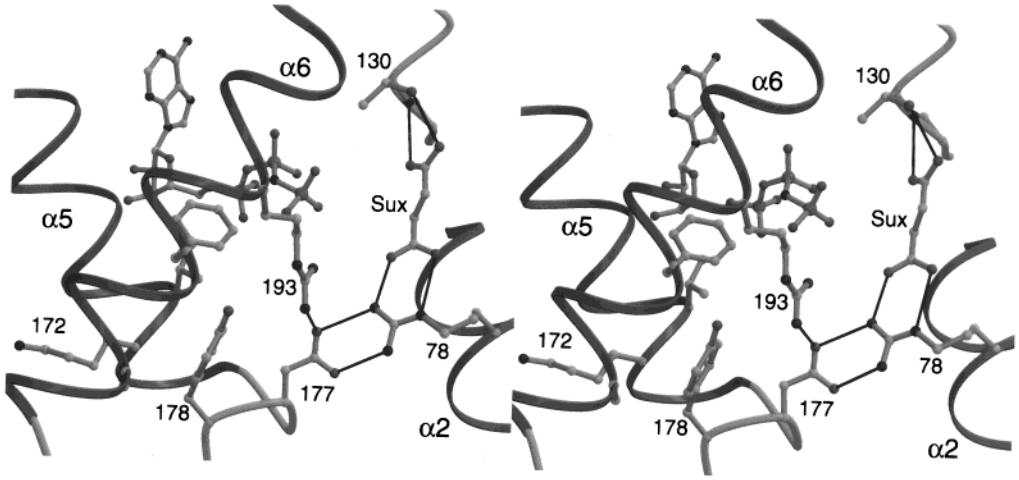

FIGURE 5: Interconnection of the ATP and F6P binding loops via Asp177 and Arg78. This stereodiagram illustrates the F6P and ATP binding region of the RT2K-Wo/*C*2 6-PF-2-K domain, and the link between the ATP and F6P binding loops. Succinate (Sux) is shown bound in the F6P binding pocket, interacting with Arg78. The ATP that is visible in the back of the figure is included to reinforce the proximity of the two binding sites (derived from the RT2K-Wo/$P3_121$ structure; recall that the RT2K-Wo/*C*2 structure has an empty ATP binding pocket). Asp177 and Arg78 are part of the ATP and F6P binding loops, respectively. The salt bridge between them links the two loops together, and has been observed in all four 6-PF-2-K domains. Asp177 and Tyr178 together are found near the tip of the ATP binding loop (labeled 177 and 178). Note their proximity to Lys172, here shown in the switched-out conformation that occurs in the absence of an ATP γ-phosphate. Changes in the conformation of this switch helix could easily be communicated to the F6P binding pocket via the F6P binding side chain of Arg78. Thus, the state of the ATP binding site could be communicated to the F6P site.

the kinetics of 6-PF-2-K activity in wild type and mutant proteins showed that Lys172 is important for catalysis, but not ATP binding (*20*). The extensive data for the G-proteins (*8*, *11*, *13*, *14*), together with our own (*20*), implicate Lys172 and its analogues as critical catalytic residues, acting to stabilize negative charge on the $\beta-\gamma$ bridge oxygen and/or the γ-phosphate during the life of the transition state. The existence of the helical switch motion of Lys172 is an unexpected parallel between the 6-PF-2-K domain and the heterotrimeric G-proteins, where a switch motion of Arg178 is part of the GTP signaling mechanism (*45*). The potential of the 6-PF-2-K switch motion to play a role in 6-PF-2-K regulation, beyond its direct role in catalysis and substrate−product exchange, will be developed below.

Succinate Binding and the Interconnection of the ATP and F6P Binding Loops. There are a series of interactions that connect the ATP and F6P binding loops, shown in Figure 5 for H256A-B. Recall that succinate interacts with Arg78 in the F6P binding loop, a residue that we have shown by mutagenesis to be critical to F6P binding (*20*). Arg78 in turn interacts with Asp177 in a bidentate salt bridge. Asp177 also interacts with Arg193, another critical F6P binding residue (*20*). This same constellation of interactions appears in all four of the 6-PF-2-K structures. Asp177 is at the C-terminal end of helix α5, which is the helix that undergoes the ATP-dependent switch transition. The turn between helices α5 and α6 is the tip of the ATP binding loop, but as we have just described, the interactions of Asp177 with critical F6P-binding residues suggest an important role for this region in F6P binding as well. Thus, we have analyzed the kinetics of several enzymes mutated in this region ($_{174}$GSPDY$_{178}$), and the results are presented in Table 3. As expected, none of these 6-PF-2-K domain mutations had a significant impact on Fru-2,6-P_2ase activity (data not shown). Further, mutations of Gly174, Ser175, and Pro176 had little or no effect on 6-PF-2-K activity (data not shown). In contrast, mutations of Asp177 and Tyr178 had a significant impact on 6-PF-2-K activity, primarily through an effect on K_m^{F6P}. These results clearly demonstrate the importance of the salt bridge between Asp177 and Arg78, and reveal a dependence on a large hydrophobic residue at position 178.

Table 3: Kinetic Constants of 6-PF-2-K Activity of RT2K-Wo and Mutant Enzymes[a]

enzyme	k_{cat} (s^{-1})	K_{ATP} (mM)	k_{cat}/K_{ATP} (M^{-1} s^{-1})	fold decrease	K_{F6P} (mM)	k_{cat}/K_{F6P} (M^{-1} s^{-1})	fold decrease
WT	0.073	0.10	730		0.04	1800	
D177N	0.043	1.00	43	17	3.7	12	150
Y178F	0.083	1.50	55	13	1.4	59	31
Y178S	0.100	0.80	130	5.6	28	3.6	500
Y178K	0.016	2.30	6.8	107	27	0.58	3103

[a] K_{ATP} was determined with the following F6P concentrations: 20 mM Y178K, 20 mM Y178S, 15 mM D177N, 5 mM Y178F, all others at 2 mM. K_{F6P} was determined at 5 mM ATP.

Inspection of Figure 5 shows that Y178 is part of a local hydrophobic core formed by residues in the ATP binding loop and extending to the P-loop region (not visible in Figure 5). This local hydrophobic pocket and the interaction of Asp177 of the ATP binding loop with Arg78 of the F6P binding loop link the two substrate binding loops into an apparently stable structure. The fact that we only observe minor changes in the positions of the ATP and F6P binding loops (compared to the large motions observed in adenylate kinase) even in the absence of either substrate (no ATP or F6P in RT2K-Wo/*C*2) suggests that the 6-PF-2-K domain does not undergo large-scale rearrangements during its catalytic cycle. This is supported by the interconnection of the ATP and F6P binding loops, and the sensitivity of catalytic activity to changes in this region despite no likely direct role in catalysis. Our results also clearly establish a direct functional connection between the ATP and F6P binding loops. First, the mutagenesis data reported here establish the importance of the interactions surrounding Asp177. We have also noted in previous work (*17*, *20*) that several mutations that should only affect ATP binding (i.e., Lys51, Thr52, Asp128, and K172) also have a profound impact on F6P binding. As an example, the mutation of

Lys172 to alanine resulted in an enzyme with a 240-fold reduction in V_{max}, a 1000-fold reduction in V/K_{ATP}, and an unexpected 14000-fold reduction in V/K_{F6P} (*20*). There are at least two explanations for this observation; the ATP molecule itself could be a ligand for F6P binding, or a reorganization of the active site that promotes F6P binding occurs upon ATP binding.

We believe that the switch motion of Lys172 is one such candidate for a reorganization of the ATP loop that could promote F6P binding. The reorganization of the switch helix could alter the binding capacity of the F6P binding pocket through the interaction of Asp177 with the critical F6P-binding residues, Arg78 and Arg193. In our comparison of these structures, we do not see evidence of a wholesale reorganization of the F6P binding site that correlates with the switch motion. The current X-ray data would not, however, reveal any changes in the dynamics of the F6P binding site due to the alteration of the switch helix. It is noteworthy that in the RT2K-Wo/$P3_121$ structure (where K172 is switched into the ATP binding site), succinate was not bound at a significant level, despite the fact that it was included in the crystallization at the same concentration used in the RT2K-Wo/*C*2 crystallization, where the succinate is found at full occupancy. Thus, the level of succinate binding to the F6P binding site correlates with the state of the switch helix, an indirect indicator that F6P binding is also likely affected.

Summary. The structures and kinetic data presented in this paper provide several new insights into the function of the 6-PF-2-K domain of the 6-PF-2-K/Fru-2,6-P_2ase bifunctional enzyme. We have shown specific binding of succinate to the F6P binding site, and demonstrated a specific inhibition of 6-PF-2-K activity that may suggest a mechanism of feedback inhibition of 6-PF-2-K activity via citric acid cycle intermediates. The increased glycolytic activity associated with Fru-2,6-P_2 stimulation of PFK leads to increased concentrations of citric acid cycle intermediates. It is possible that an increased cytosolic concentration of succinate (or possibly any of the tri- or dicarboxylate intermediates, malate, citrate, isocitrate, fumarate, etc.) could then act to suppress 6-PF-2-K activity, in turn suppressing glycolysis. Succinate enters the cytosol from the mitochondria by exchange with cations (*46*), and while the literature is sparse with respect to measurements of cytosolic concentrations of citric acid cycle intermediates, succinate concentrations have been reported in the micromolar to millimolar range (*43*, *47*, *48*). Thus, there is significant potential for a physiologically relevant role for the observed succinate inhibition of F6P binding to the 6-PF-2-K domain. Similarly, the binding of β-OG in a position that could interfere with F6P binding suggests a possible role for fatty acids as inhibitors of 6-PF-2-K activity.

The most striking finding in this study, however, is the ATP-dependent rearrangement in the ATP binding loop that is reminiscent of the switch motions observed for the heterotrimeric G-proteins. This rearrangement certainly has consequences for the mechanism of catalysis and the mechanism of substrate binding and product release. Through the interconnection of the ATP and F6P binding loops via Asp177, this switch motion may also communicate the nature of the ligand in the ATP binding site to the F6P binding site, leading to an ordered binding of substrates to the 6-PF-2-K domain. We have provided kinetic data for mutant enzymes that are consistent with this communication between the ATP and F6P binding loops. While these results yield valuable insights, we still seek to determine structures of the enzyme that include bound F6P, transition state mimics, and the N-terminus of the enzyme. Only then can we build a complete picture of the mechanisms of catalysis and regulation in this important bifunctional regulatory enzyme.

ACKNOWLEDGMENT

We thank Cu Nguyen, Yang Li, and Lori Neil for excellent technical assistance.

REFERENCES

1. Uyeda, K. (1991) in *Study of Enzymes II* (Kuby, S. A., Ed.) pp 445−456, CRC Press, Boca Raton, FL.
2. Pilkis, S. J., Claus, T. H., Kurland, I. J., and Lange, A. J. (1995) *Annu. Rev. Biochem. 64*, 799−835.
3. Rousseau, G. G., and Hue, L. (1993) *Prog. Nucleic Acid Res. Mol. Biol. 45*, 99−127.
4. Hasemann, C. A., Istvan, E. S., Uyeda, K., and Deisenhofer, J. (1996) *Structure 4*, 1017−1029.
5. Walker, J. E., Saraste, M., Runswick, M. J., and Gay, N. J. (1982) *EMBO J. 1*, 945−951.
6. Diederichs, K., and Schulz, G. E. (1991) *J. Mol. Biol. 217*, 541−549.
7. Pai, E. F., Krengel, U., Petsko, G. A., Goody, R. S., Kabsch, W., and Wittinghofer, A. (1990) *EMBO J. 9*, 2351−2359.
8. Coleman, D. E., Berghuis, A. M., Lee, E., Linder, M. E., Gilman, A. G., and Sprang, S. R. (1994) *Science 265*, 1405−1412.
9. Shirakihara, Y., and Evans, P. R. (1988) *J. Mol. Biol. 204*, 973−994.
10. Knowles, J. R. (1980) *Annu. Rev. Biochem. 49*, 877−919.
11. Maegley, K. A., Admiraal, S. J., and Herschlag, D. (1996) *Proc. Natl. Acad. Sci. U.S.A. 93*, 8160−8166.
12. Admiraal, S. J., and Herschlag, D. (1996) *Chem. Biol. 2*, 729−739.
13. Sondek, J., Lambright, D. G., Noel, J. P., Hamm, H. E., and Sigler, P. B. (1994) *Nature 372*, 276−279.
14. Schweins, T., Geyer, M., Scheffzek, K., Warshel, A., Kalbitzer, H. R., and Wittinghofer, A. (1995) *Nat. Struct. Biol. 2*, 36−44.
15. Tesmer, J. J., Berman, D. M., Gilman, A. G., and Sprang, S. R. (1997) *Cell 89*, 251−261.
16. Zor, T., Bar-Yaacov, M., Elgavish, S., Shaanan, B., and Selinger, Z. (1997) *Eur. J. Biochem. 249*, 330−336.
17. Uyeda, K., Wang, X.-L., Mizuguchi, H., Li, Y., Nguyen, C., and Hasemann, C. A. (1997) *J. Biol. Chem. 272*, 7867−7872.
18. Scheffzek, K., Ahmadian, M. R., Kabsch, W., Wiesmuller, L., Lautwein, A., Schmitz, F., and Wittinghofer, A. (1997) *Science 277*, 333−338.
19. Rittinger, K., Walker, P. A., Eccleston, J. F., Smerdon, S. J., and Gamblin, S. J. (1997) *Nature 389*, 758−762.
20. Mizuguchi, H., Cook, P. F., Hasemann, C. A., and Uyeda, K. (1997) *Biochemistry 36*, 8775−8784.
21. Watanabe, F., Jameson, D. M., and Uyeda, K. (1996) *Protein Sci. 5*, 904−913.
22. Tauler, A., Lin, K., and Pilkis, S. J. (1990) *J. Biol. Chem. 265*, 15617−15622.
23. Mizuguchi, H., Cook, P. F., Tai, C.-H., Hasemann, C. A., and Uyeda, K. (1999) *J. Biol. Chem. 274*, 2166−2175.
24. Yuen, M. H., Mizuguchi, H., Lee, Y.-H., Cook, P. F., Uyeda, K., and Hasemann, C. A. (1999) *J. Biol. Chem. 274*, 2176−2184.
25. Tominaga, N., Minami, Y., Sakakibara, R., and Uyeda, K. (1993) *J. Biol. Chem. 268*, 15951−15957.
26. Istvan, E. S., Hasemann, C. A., Kurumbail, R. G., Uyeda, K., and Deisenhofer, J. (1995) *Protein Sci. 4*, 2439−2441.
27. Kunkel, T. (1985) *Proc. Natl. Acad. Sci. U.S.A. 82*, 488−492.

28. Sakata, J., Abe, Y., and Uyeda, K. (1991) *J. Biol. Chem. 266*, 15764−15770.
29. Sanger, F., Nicklen, S., and Coulson, A. (1977) *Proc. Natl. Acad. Sci. U.S.A. 74*, 5463−5467.
30. Penefsky, H. (1977) *J. Biol. Chem. 252*, 2891−2899.
31. Furuya, E., and Uyeda, K. (1981) *J. Biol. Chem. 256*, 7109−7112.
32. Uyeda, K., Furuya, E., and Luby, L. J. (1981) *J. Biol. Chem. 256*, 8394−8399.
33. Otwinowski, Z., and Minor, W. (1997) *Methods Enzymol. 276*, 307−326.
34. Brünger, A. T. (1993) in *X-PLOR Version 3.1: A system for crystallography and NMR*, Yale University Press, New Haven, CT.
35. Collaborative Computational Project, Number 4 (1994) *Acta Crystallogr. D50*, 760−763.
36. Brünger, A. T. (1992) *Nature 355*, 472−475.
37. Read, R. J. (1986) *Acta Crystallogr. A42*, 140−149.
38. Jones, T. A., Bergdoll, M., and Kjeldgaard, M. (1990) in *Crystallographic and modeling methods in molecular design* (Bugg, C. E., and Ealick, S. E., Eds.) pp 189−199, Springer-Verlag, New York.
39. Bernstein, F. C., Koetzle, T. F., Williams, G. J. B., Meyer, E. F., Brice, M. D., Rodgers, J. R., Kennard, O., Shimanouchi, T., and Tasumi, M. (1977) *J. Mol. Biol. 112*, 535−542.
40. Tsujikawa, T., Watanabe, F., and Uyeda, K. (1995) *Biochemistry 34*, 6389−6393.
41. Schulz, G. E., Müller, C. W., and Diederichs, K. (1990) *J. Mol. Biol. 213*, 627−630.
42. Muller, C. W., Schlauderer, G. J., Reinstein, J., and Schulz, G. E. (1996) *Structure 4*, 147−156.
43. Iles, R. A., Barnett, D., Strunin, L., Strunin, J. M., Simpson, B. R., and Cohen, R. D. (1972) *Clin. Sci. 42*, 35−45.
44. Müller-Dieckmann, H.-J., and Schulz, G. E. (1995) *J. Mol. Biol. 246*, 522−530.
45. Sprang, S. R. (1998) *Curr. Opin. Struct. Biol. 7*, 849−856.
46. Van Rossum, G. D. (1969) *Arch. Biochem. Biophys. 133*, 373−384.
47. Goldberg, N. D., Passonneau, J. V., and Lowry, O. H. (1966) *J. Biol. Chem. 241*, 3997−4003.
48. Cascarano, J., Ades, I. Z., and O'Conner, J. D. (1976) *J. Exp. Zool. 198*, 149−153.
49. Kraulis, P. J. (1991) *J. Appl. Crystallogr. 24*, 946−950.
50. Esnouf, R. M. (1997) *J. Mol. Graphics Modell. 15*, 132−134.
51. Merritt, E. A., and Murphy, M. E. P. (1994) *Acta Crystallogr. D50*, 869−873.

BI991268+